INORGANIC CHEMISTRY

FRONTIERS

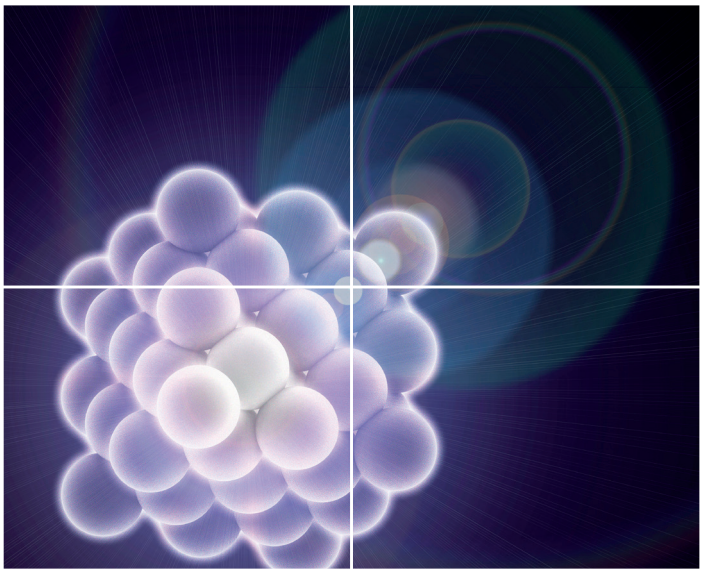

Accepted Manuscript

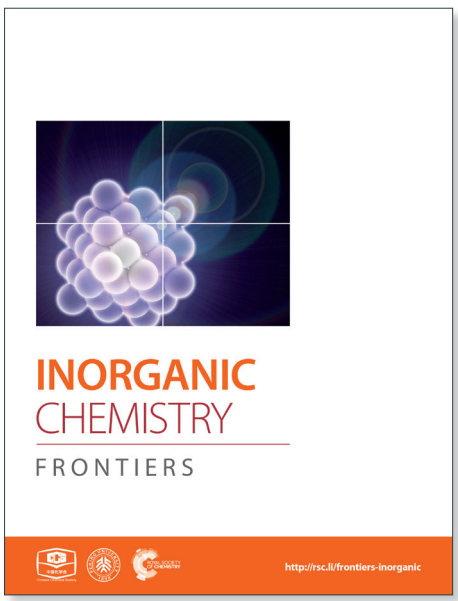

This is an *Accepted Manuscript*, which has been through the Royal Society of Chemistry peer review process and has been accepted for publication.

Accepted Manuscripts are published online shortly after acceptance, before technical editing, formatting and proof reading. Using this free service, authors can make their results available to the community, in citable form, before we publish the edited article. We will replace this *Accepted Manuscript* with the edited and formatted *Advance Article* as soon as it is available.

You can find more information about *Accepted Manuscripts* in the **Information for Authors**.

Please note that technical editing may introduce minor changes to the text and/or graphics, which may alter content. The journal's standard **Terms & Conditions** and the **Ethical guidelines** still apply. In no event shall the Royal Society of Chemistry be held responsible for any errors or omissions in this *Accepted Manuscript* or any consequences arising from the use of any information it contains.

Journal Name Inorganic Chemistry Frontiers Dynamic Article Links ►

Cite this: DOI: 10.1039/c0xx00000x

www.rsc.org/xxxxxx

ARTICLE TYPE

In search of structure-function relationships in transition-metal based rectifiers.

Tingting Weng,[a] Daniel DeBrincat, Vaida Arcisauskaite and John E. McGrady*[c]

Received (in XXX, XXX) Xth XXXXXXXXX 20XX, Accepted Xth XXXXXXXXX 20XX
DOI: 10.1039/b000000x

Abstract

Heterometallic chains have been proposed as potential current rectifiers in molecular electronics, their left-right asymmetry providing, at least in principle, a mechanism for differentiation of current flow in forward and reverse directions. Here we compare two known extended metal atom chains (EMACs), $Ru_2Ni(dpa)_4(NCS)_2$ and $Ru_2Cu(dpa)_4(NCS)_2$, both of which meet the first criterion for rectification in so much as they are physically asymmetric. In both cases the dominant transport channel is a doubly degenerate π* orbital localised, to a first approximation, on the Ru_2 unit. As a result, current is limited by tunnelling across the Au-SCN-Ni/Cu junction. The paramagnetic Ni centre tunes the left-right delocalisation of the channel, making the minority-spin (β) channel more transparent than its spin-α counterpart and this difference provides the basis for asymmetry in the current under forward and reverse bias.

Introduction

The discipline of molecular electronics is motivated by the desire to replace the semiconductor-based components of contemporary devices with molecular-based analogues.[1] As a result, there is a great deal of interest in designing molecules which, when supported between two electrodes, may reproduce the functionality of wires, diodes and even transistors. As with all types of mimicry, even when the gross function (*viz* electronic conduction or rectification) is replicated, it is not always clear that the underlying mechanism is the same. This point is illustrated by the recent surge in literature reports of 'molecular rectifiers', components which will allow the preferential flow of current in one direction.[2,3,4,5,6,7,8,9,10,11,12,13,14] The p-n junction diode which lies at the heart of conventional semiconductor devices is the inspiration behind these studies, but to what extent do the physics and chemistry in these putative mimics really reflect the key features of the original? It is clear that the presence of *any* element of asymmetry, either in a molecule or its contact to an electrode, eliminates the possibility that current flow is *rigorously* identical in both directions. The question then becomes one of degrees: to what extent does the asymmetric perturbation impact on the observable of interest, the flow of current.

In the seminal 1974 paper[15] where they identified the potential rectifying properties of the Donor-bridge-Acceptor (D-σ-A or D-π-A) architecture (Figure 1, left), Aviram and Ratner argued that under applied bias electrons should flow preferentially from the source electrode to the vacant LUMO on the acceptor to the (filled) HOMO of the donor and finally to the drain electrode (the 'Aviram-Ratner direction'). If the acceptor and donor are identified with the p- and n-doped regions of the semiconductor, then this implies the opposite direction for facile electron transport to that observed in a p-n junction (*i.e.* from electron-poor to electron-rich regions). Indeed a later study of the Aviram-Ratner diode using density functional theory suggested that the potential drop was localised at the electrode-molecule interface, and the computed rectification ratio was low.2 The Aviram-Ratner architecture shown in Figure 1 (left) has not been realised synthetically but a number of closely related D-σ-A and D-π-A triads (Figure 1, right, for example)[4,5] have show rectification ratios of up to 60, albeit with preferential electron flow from the donor to the acceptor: *i.e.* in the '*anti* Aviram-Ratner' direction.4[a] This direction of electron flow can be understood in terms of the strength of coupling of the donor and acceptor groups to the electrodes: *i.e.* the extent to which the orbitals localised on these two units follow the potential of the source or drain. In Aviram and Ratner's model, the Fermi levels of the electrodes are raised or lowered relative to fixed HOMO (D) or LUMO (A) energies, with the result that electrons flow in the A→D direction (Figure 1, left). If, in contrast, the HOMO of the donor and the LUMO of the acceptor are strongly coupled to their neighbouring electrodes, the HOMO of the donor can be driven above the LUMO of the acceptor and electron flow is then in the *anti* Aviram-Ratner direction (Figure 1, right). These bias-induced shifts in zeroth-order energy levels can lead to dramatic changes in left-right delocalisation of the channel, particularly when the levels come into resonance.

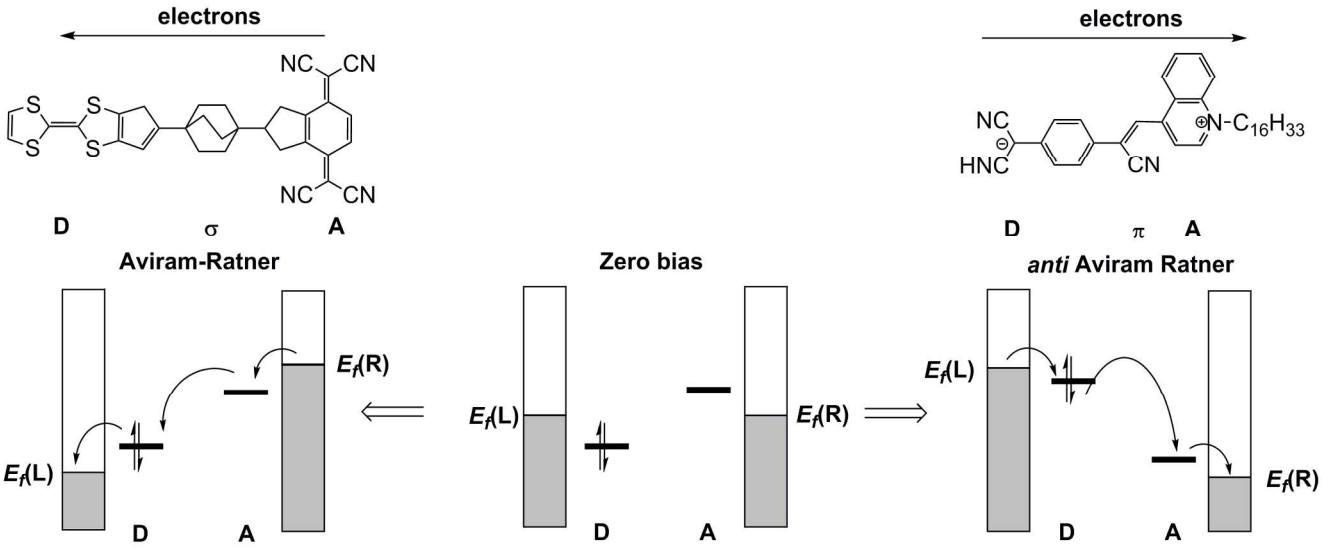

Figure 1. Current flow in the Aviram-Ratner (left) and anti-Aviram-Ratner directions in molecular rectifiers.

Much of the recent progress in molecular electronics has come in the context of organic systems where a conjugated π system provides the dominant transport channel. However arrays of transition metal ions have much to offer,[16] not least because the relative lability of the coordinate bond provides a potent tool for custom design of molecules. The so-called Extended Metal Atom Chains (EMACs), arrays of transition metal ions supported by polydentate ligands, are a case in point: advances in synthetic technique mean that it is now possible to vary systematically both their length (3 – 11 metal atoms) and composition.[17] The major barrier to the full exploitation of these systems is the lack of clear correlations between structure and function, function in this case being the ability to support current flow. Such models are relatively well established in organic electronics where the relationship between the properties of the frontier π orbital domain and current flow is well understood.[18,19] The situation is less clear-cut in transition metal ions because the generally poor d-d overlap and strong electron-electron repulsions can lead to a densely populated window around the Fermi level. Systematic trends in conductance have begun to emerge through the experimental measurements of Peng, Hsien and co-workers, who have established its dependence on composition (Cr_3, Co_3, Ni_3, Ru_3),[20] on chain length (M_3, M_5)[21] and also on the valency of the metals ($[Ni_5]^{10+}$, $[Ni_5]^{8+}$). [22] At the same time we [23] and others[24,25,26] have begun to explore these properties from a theoretical perspective.

In this paper we address a simple question: what electronic features of an extended metal atom chain do we need to take into account when designing an effective molecular rectifier? As a platform for this study we choose a pair of molecules, $Ru_2Ni(dpa)_4(NCS)_2$ and $Ru_2Cu(dpa)_4(NCS)_2$ shown in Figure 2 (dpa = dipyridylamido), the chloride-capped analogues of which have been synthesised by Peng and co-workers.[27] The authors noted that both molecules meet the first requirement of rectification, in so much as they are obviously asymmetric. Moreover, they are somewhat unusual in the context of EMAC chemistry in that their ground states are best formulated as $\{Ru_2\}^{5+}$ M^{1+} (M = Ni, Cu) rather than the more common isovalent $\{M^{2+}\}_3$. The charge separation reflects the substantial electronic differences between late first row (Ni, Cu) and mid second row (Ru) transition metal ions, and suggests that the molecular orbitals should be spatially localised on one side or the other. This, in turn, should offer the potential for substantial current rectification, but which of the two is more effective?

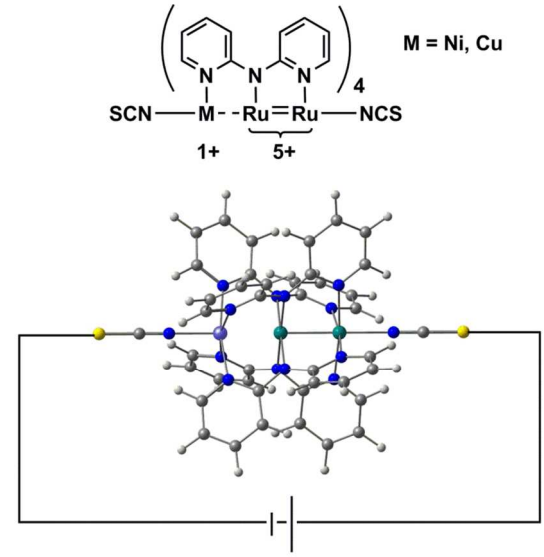

Figure 2. Structure of an asymmetric EMAC, $Ru_2M(dpa)_4(NCS)_2$.

Computational methods

All calculations of the gas-phase electronic structure of $Ru_2M(dpa)_4(NCS)_2$, M=Ni, Cu were performed using the Amsterdam Density Functional package ADF2012[28] package. A double-ζ Slater-type basis set, extended with a single polarization function (DZP) was used to describe the main group atoms, while ruthenium, copper and nickel were modeled with a triple-ζ basis set with a single polarization function (TZP). Electrons in orbitals

up to and including 1s {C, N}, 2p{S}, 2p {Ni,Cu} and 3d {Ru} were considered part of the core and treated in accordance with the frozen core approximation. The local density approximation was employed for the optimizations, [29] along with the local exchange-correlation potential of Vosko, Wilk and Nusair[30] and gradient corrections to exchange and correlation proposed by Perdew, Becke and Ernzerhof (PBE).[31] Scalar relativistic effects were introduced through the zeroth order relativistic approximation (ZORA) Different configurations were defined using the 'occupations' key. Transport calculations were performed with the ATK12.8.2 [32, 33] package using the LDA functional with the self-interaction correction (SIC) of Perdew and Zunger (LSDA.PZ).[34] The methodology combines a density functional theory treatment of the electronic structure with the Keldysh non-equilibrium Green's function approach to simulating coherent transport.[35] The scattering region contained the EMAC sandwiched between 6 x 6 layer of the Au (111) surface of the source and the drain, respectively. The sulfur atoms of the two NCS^- ligands are located in a hollow site on the Au (111) surface with Au-S distance 2.52 Å. The precise details of the contact geometry remain a significant issue in all transport calculations – the 'hollow-site' geometry with a gold-sulfur distance of 2.52 Å (corresponding to a distance of ~1.9 Å between the sulfur and the surface) adopted here has been established as the global minimum for many examples of sulfur coordination to Au (111) [36] and is used in the majority of comparative studies.[37] A double-ζ basis set, extended with single polarization function, (DZP) was used to describe all atoms except gold which was modelled using a single-ζ basis set, extended with single polarization function, (SZP). Core electrons were described by norm-conserving pseudopotentials. [38] The electronic structure of the two-probe systems at equilibrium was converged using a 100 Ry mesh cut-off, finite temperature of 300K at the electrodes. Sampling of the Brillouin zone was performed using a Monkhorst-Pack grid [39] with 100 k-points along the transport direction. In the calculation of the transmission spectra and currents, a 5 x 5 grid was used to sample the Brillouin zone, and the bias window was sampled at 0.01 eV intervals. The initial spin density for the two-probe calculations was polarized to be consistent with the net spin densities of the isolated molecules in their gas phase ground states. A full set of cartesian coordinates for the two-probe system is provided in the supporting information (Table S1).

Results and Discussion

Electronic structure at equilibrium.

With only minor caveats, the picture of the ground state electronic structure of $Ru_2Ni(dpa)_4(NCS)_2$ in the gas phase that emerges from our calculations is consistent with the previously published model of Bénard, Rohmer and Peng which predicts a quintet ground state (S = 2).[27] The only significant difference is that the perfectly linear (C_4 symmetric) Ru_2Ni array proves not to be a minimum on the potential energy surface of $Ru_2Ni(dpa)_4(NCS)_2$: a bent structure with an Ru-Ru-Ni angle of approximately 172° is marginally (0.05 eV) more stable (Table 1). We return to a discussion of the bending and its origins later, but as it has little impact on the electronic structure, at least to first order, we focus the discussion below on the less stable linear isomer. As shown by Bénard, the ground state of $Ru_2Ni(dpa)_4(NCS)_2$ is best formulated as Ni^{1+}-$\{Ru_2\}^{5+}$ rather than Ni^{2+}-$\{Ru_2\}^{4+}$: the Mulliken charges are 0.45, 1.38 and 1.19 for Ni, Ru_c and Ru_t, respectively (Ru_c and Ru_t denote central and terminal, ruthenium centres, respectively) and the Mulliken spin density of 1.08 at nickel is more consistent with a d^9 configuration (Ni^{1+}) than d^8 (Ni^{2+}). The presence of vacancies in the spin-β components of the Ni-N σ* ($d_{x^2-y^2}$) and the Ru-Ru π* and δ* orbitals is apparent in the Kohn-Sham molecular orbital diagram shown in Figure 3(a). The critical left (Ni)-right (Ru_2) localisation of the orbitals of π and δ symmetry is apparent in contour plots in Figure 3. In contrast the orbitals of σ symmetry show appreciable left-right delocalisation, with the σ^{nb} orbital having almost equal amplitudes on Ni d_{z^2} and Ru_t d_{z^2}. The splitting between the spin-α and spin-β components of the different orbitals is particularly relevant to the subsequent discussion of electron transport: the smaller separation between the $\pi^*_{\alpha/\beta}$ levels (~0.6 eV) relative to Ni $d_{xz/yz\ \alpha/\beta}$ (~0.8 eV) reflects the stronger electron-electron repulsions in the smaller 3d orbital.

Journal Name

Dynamic Article Links ►

Cite this: DOI: 10.1039/c0xx00000x

www.rsc.org/xxxxxx

ARTICLE TYPE

Table 1. Computed bond lengths (Å) and angles Ru-Ru-M (◦), M = Ni, Cu, Mulliken charges (Q) and spin densities (ρ) and relative energies (eV) of $Ru_2Ni(dpa)_4(NCS)_2$ and $Ru_2Cu(dpa)_4(NCS)_2$ in both linear (C_{4v}) and bent (C_1) geometries. X-ray data for the $Ru_2M(dpa)_4Cl_2$ are shown for comparison.[22]

	M-Ruc	Ruc-Rut	θ	M-N	Ru_c-N	Ru_t-N	Q(M)	Q(Ru_c)	Q(Ru_t)	ρ(M)	ρ(Ru_c)	ρ(Ru_t)	E/eV
$Ru_2Ni(dpa)_4(NCS)_2$ (C_{4v})	2.43	2.37	180	4 x 2.13	4 x 2.07	4 x 2.14	0.45	1.38	1.19	1.08	1.28	0.82	0.0
$Ru_2Ni(dpa)_4(NCS)_2$ (C_1)	2.44	2.38	172.2	2.07-2.23	2.04-2.12	2.10-2.18	0.47	1.37	1.20	1.17	1.23	0.75	-0.05
$Ru_2Ni(dpa)_4Cl_2$[†]	2.349(5)	2.341(4)	180	2.102(3)	2.012(3)	2.106(3)							
$Ru_2Cu(dpa)_4(NCS)_2$ (C_4)	2.60	2.35	180	4 x 2.24	4 x 2.08	4 x1.14	0.29	1.47	1.20	0.16	1.35	0.86	0.0
$Ru_2Cu(dpa)_4Cl_2$	2.575(3)	2.246(3)	180	2.173(6)[‡]	2.046(2)	2.136(4)							

[†] The terminal Ru and Ni positions in this data set could not be distinguished: the authors note that actual uncertainties in bond lengths are likely to be much higher. [‡] This value represents the average of four distinct Cu-N bond lengths varying between 2.126 and 2.226 Å.

Cite this: DOI: 10.1039/c0xx00000x

www.rsc.org/xxxxxx

ARTICLE TYPE

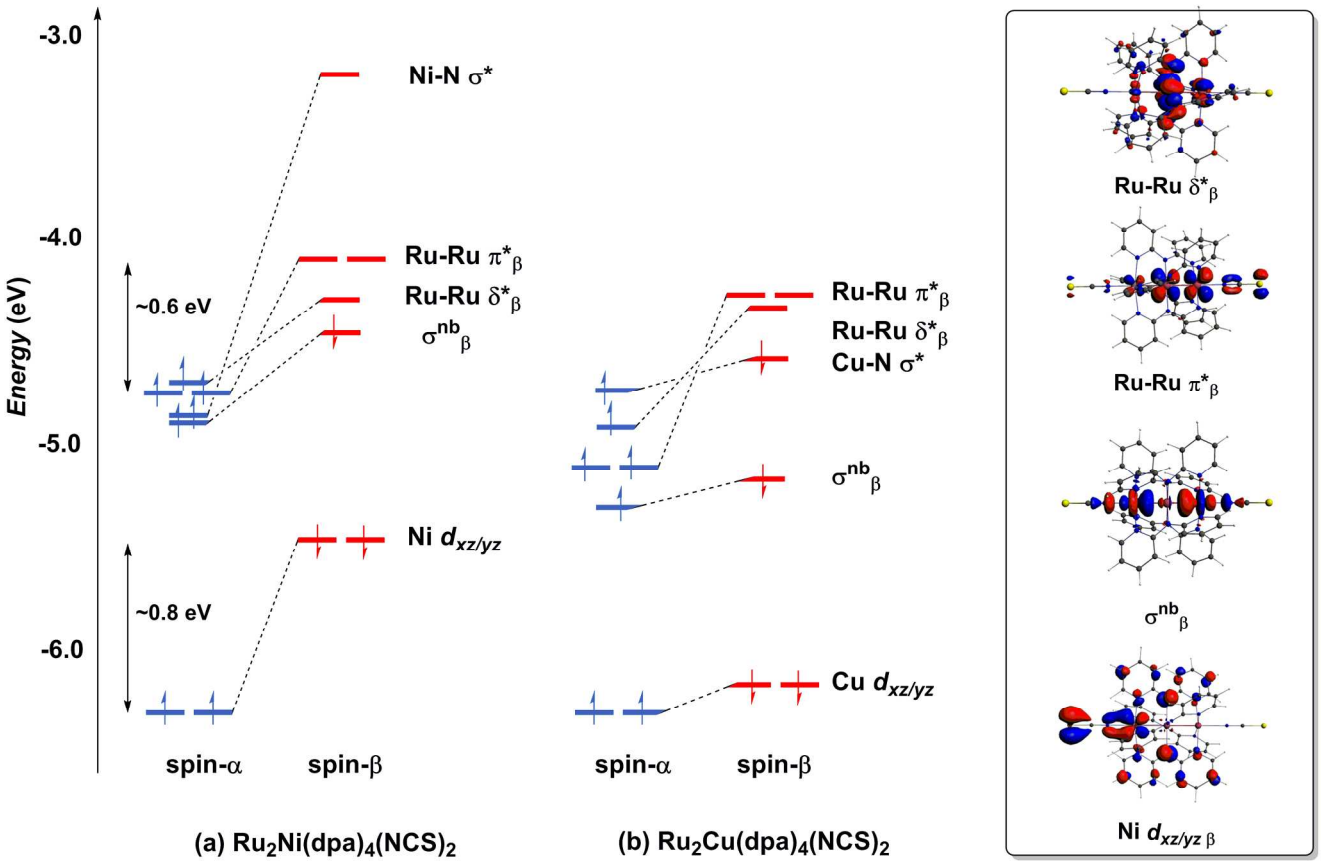

Figure 3. Comparison of the frontier Kohn-Sham orbitals (a) for $Ru_2Ni(dpa)_4(NCS)_2$ and (b) for $Ru_2Cu(dpa)_4(NCS)_2$. Contour plots are shown for the $Ru_2Ni(dpa)_4(NCS)_2$ case.

The tendency for the $Ru_2Ni(dpa)_4(NCS)_2$ species to bend can be traced to the energetic proximity of the occupied σ^{nb}_{β} orbital to the vacant π^*_{β}: removing the axial symmetry allows the two to mix, further stabilising the lower-lying orbital (a second order Jahn-Teller distortion). The bending of the Ru_2Ni framework also introduces a significant variation in the Ni-N bond lengths (computed values vary between 2.07 and 2.23 Å). It is difficult to validate the prediction of bending against experimental data due to the disorder in the crystal structure of $Ru_2Ni(dpa)_4(Cl)_2$, but it is possible that the bending is in fact the source of the disorder. What is clear is that the closely related homometallic Ru_3 chains are strongly bent for all but the most electron donating terminal ligands, and for very similar electronic reasons.[23d]

Turning to the copper analogue $Ru_2Cu(dpa)_4(NCS)_2$, the Cu 3d manifold is now stabilised (relative to Ni) due to the increase in effective nuclear charge and both spin components of the Cu-N σ* orbital are now occupied (Cu^{1+}, d^{10}). This has several consequences for the molecular orbital array, the most obvious being that the distinction between the spin-α and spin-β components of Cu $d_{xz/yz}$ is much reduced compared to $Ru_2Ni(dpa)_4(NCS)_2$. Moreover, the σ^{nb} orbital, with similar amplitudes on Cu and Ru_t, is stabilised relative to the Ru-Ru π* and δ* orbitals which have only relatively minor contributions from the heterometal. The increased σ^{nb}-π* separation reduces the driving force for the bending distortion, and in fact we have been unable to locate a bent local minimum in the $Ru_2Cu(dpa)_4(NCS)_2$ case: all attempts reverted back to the linear structure. This observation is consistent with the fact that disorder problems were less acute in the crystal structure determination in this case, although the residual variation within the experimental Cu-N bond lengths (2.126-2.226 Å) suggests that the potential energy surface for the bending remains flat.

The electronic structure model developed for the gas phase persists in the device configuration where the molecules are supported between the (111) faces of two bulk gold electrodes (Figure 4(a,b)). The Mulliken spin densities on the metal centres

in $Ru_2Ni(dpa)_4(NCS)_2$, for example, are very similar to those in the gas-phase (1.15, 1.22 and 0.66 for Ni, Ru_c and Ru_t, respectively compared to values of 1.08, 1.28 and 0.82 in Table 1). The zero-bias transmission spectrum of $Ru_2Ni(dpa)_4(NCS)_2$ shown in Figure 4(a) further emphasises the close relationship between the molecule in isolation and *in situ* between the electrodes: there is a near one-to-one correspondence between the Kohn-Sham eigenvalues of the isolated molecule (Figure 3a) and the position of the resonances in the transmission spectrum. The corresponding transmission spectrum calculated using the PBE functional is shown in supporting information, Figure S2.

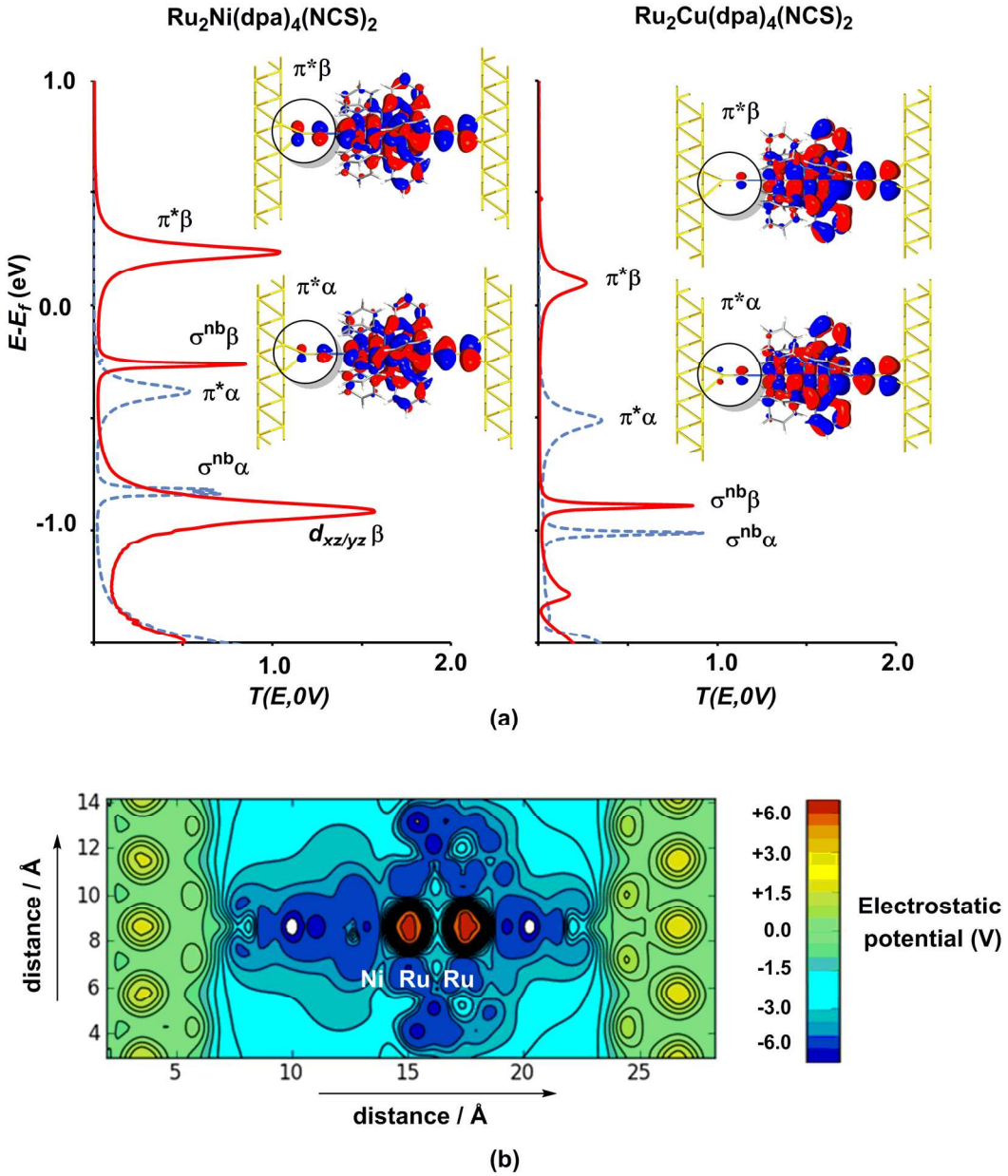

Figure 4.Equilibrium electronic structure of $Ru_2M(dpa)_4(NCS)_2$ in the device configuration where the molecule is supported between the (111) faces of two bulk gold electrodes: (a) zero-bias transmission spectrum and (b) electrostatic difference potential between the self consistent density and that of free atoms. Note that in (a) spin-α levels/channels are shown in blue, spin-β levels/channels in red. All isosurfaces are shown at the same contour level (0.008 au)

The connection between current flow and the underlying electronic structure is established through the voltage- and energy-dependent transmission function, $T(E,V)$.[40]

$$I_{\alpha/\beta} = \frac{e}{h}\int_{-\infty}^{\infty} T_{\alpha/\beta}(E,V)\big(f_L(E,V) - f_R(E,V)\big)dE \qquad \text{Equ (1)}$$

Where $f_L(E,V)$ and $f_R(E,V)$ are the Fermi functions of the left and right electrodes, respectively. The transmission function is computed through:

$$T(E,V) = tr\left[\Gamma_L G_M^{R\dagger} \Gamma_R G_M^R\right] \qquad \text{Equ (2)}$$

where G_M^R is the retarded Green's function of the molecular region. Assuming the electrode establishes contact only through the two terminal atoms of the molecule (in this case the sulfur atoms of the left and right NCS ligands), the transmission function can be approximated by:

$$T(E,V) \propto \sum_n \frac{\Gamma^2 \left(c_{SL_n} c_{SR_n}\right)^2}{(E-\varepsilon_n)^2+\Gamma^2} \qquad \text{Equ (3)}$$

where ε_n is the eigenvalue of the *n*th molecular orbital and c_{SL_n}, c_{SR_n} are the coefficients of this orbital at the left and right sulphur atoms. Γ is the imaginary part of the self energy of the electrode which has the effect of broadening the resonance. Equation 3 establishes the critical point that the degree of left-right delocalisation, encapsulated in the product of coefficients $c_{SL_n} c_{SR_n}$, determines the magnitude of the transmission function and hence, through Equation 1, the current. The current is then effectively limited by the size of the smaller of these two coefficients.

The most significant features of Figure 4 from an electron transport perspective are the channels which lie close to the Fermi level at zero bias, namely the spin-α and spin-β components of the π* channel which, to a first approximation, are localised on the Ru_2 unit and therefore couple more strongly to the right hand electrode (*i.e.* $c_{SL_n} < c_{SR_n}$). The magnitude of the transmission is therefore limited by the value of c_{SL_n}, the coefficient on the heterometal end of the molecule: physically, entry/escape of the electron from the Ni/Cu side of the molecule onto the left hand electrode is current-limiting. The spin-β component of π* in the transmission spectrum of $Ru_2Ni(dpa)_4(NCS)_2$ is strikingly more intense than its spin-α counterpart, indicating a greater degree of left-right delocalisation in the former, a point confirmed by the circled regions in the isosurface plots shown in Figure 4(a). The spatial difference between π^*_α and π^*_β is undeniably small, but it is responsible for a significant increase in transmission. In $Ru_2Cu(dpa)_4(NCS)_2$, in contrast, it is the lower lying spin-α component of the π* channel that carries the greater intensity, although the difference is less marked in this case. The spin dependence of the delocalisation of the π* channels can be understood in qualitative terms using the spin polarised molecular orbital model shown in Scheme 1. The key feature here is that the orbital arrays for the spin-α (blue) and spin-β (red) manifolds need to be constructed separately, taking account of the energies of the component orbitals (*i.e.* those on M and those on Ru_2) in zeroth order. On the left and centre of the figure are the valence orbitals of isolated Ni^{1+} ($d_{xz/yz}$) and $\{Ru_2\}^{5+}$ (Ru-Ru π*) units, respectively. In both cases the spin-α levels (blue) lie below their spin-β counterparts (red) because all three metal atoms carry positive spin density in the quintet ground state. The splitting between the spin-α and spin-β components of the $d_{xz/yz}$ orbitals on Ni^{1+} and the π* on $\{Ru_2\}^{5+}$ (shown as black double headed arrows) is determined by the magnitude of the electron-electron repulsion, which is greater on Ni than on Ru (*c.f.* the discussion of Figure 3). When the two fragments are allowed to interact, the degree of delocalisation of the π^*_α and π^*_β channels will be determined by the zeroth order splittings between the same-spin components of Ni $d_{xz/yz}$ and Ru-Ru π* (ΔE_1 and ΔE_2) in Scheme 1. As a result of the greater spin polarisation at Ni vs Ru_2, this zeroth order splitting is lowest in the spin-β manifold ($\Delta E_2 < \Delta E_1$ in Scheme 1), and the π^*_β channel is therefore the more delocalised. In effect, the Au-SCN-Ni junction is more transparent to spin-β electrons than to spin-α. In $Ru_2Cu(dpa)_4(NCS)_2$ the lower energy of the 3d orbitals on Cu reduces the degree of delocalisation, and hence the transmission, in both spin channels. Moreover, the absence of spin density on Cu (closed-shell d^{10} configuration) means that the splitting of the spin components is now *greater* in the $\{Ru_2\}^{5+}$ π* orbital than in Cu $d_{xz/yz}$. It is therefore the spin-α components that have the smaller zeroth order separation ($\Delta E_4 > \Delta E_3$) and hence the greater delocalisation (although the difference between π^*_α and π^*_β is small).

Cite this: DOI: 10.1039/c0xx00000x

www.rsc.org/xxxxxx

ARTICLE TYPE

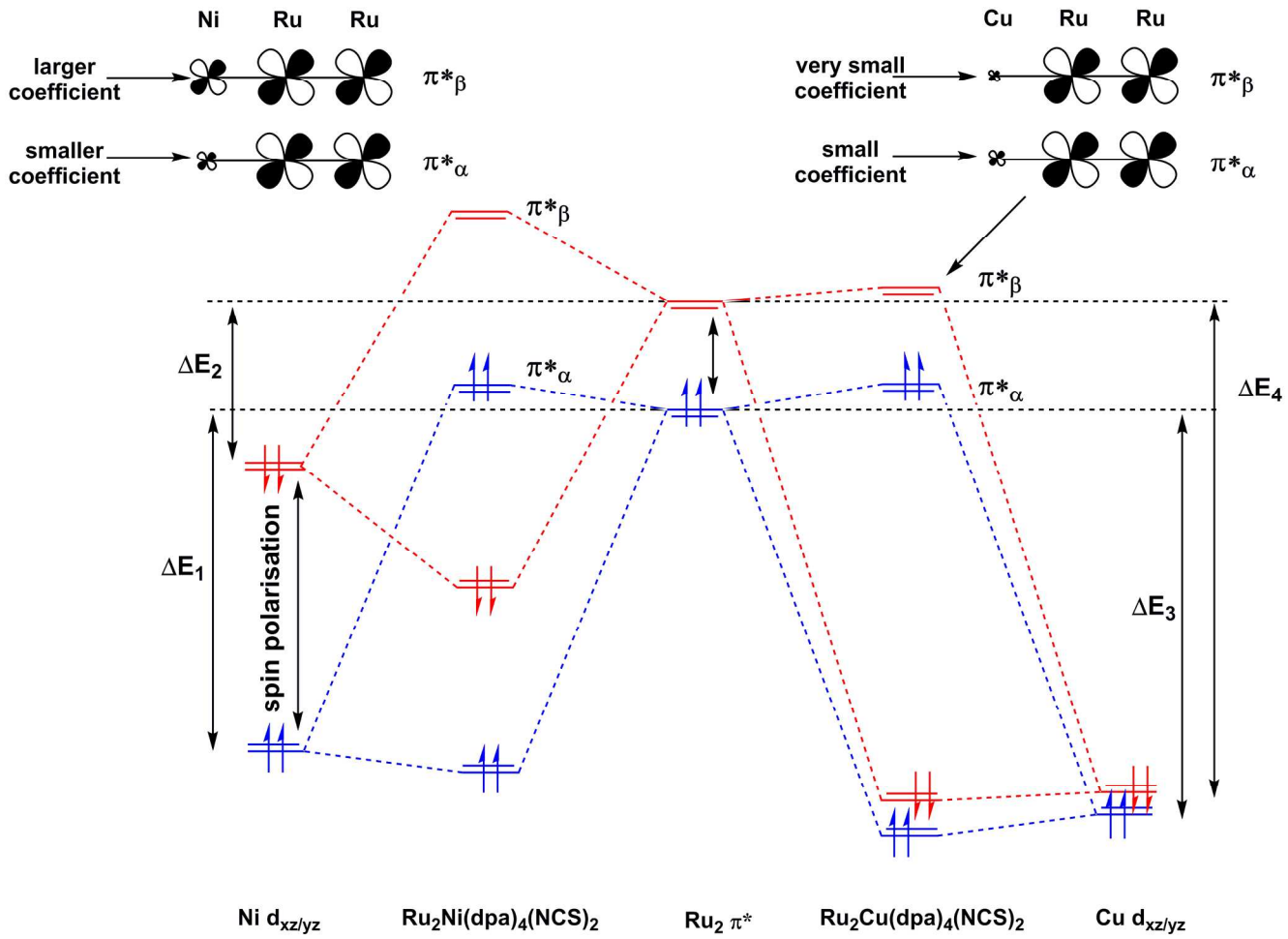

Scheme 1. Origin of the spin-dependence of the delocalisation of the π* channels in $Ru_2Ni(dpa)_4(NCS)_2$ and $Ru_2Cu(dpa)_4(NCS)_2$. Red and blue lines denote the spin-β and spin-α manifolds, respectively.

Current-voltage characteristics

The current/voltage curves for $Ru_2Ni(dpa)_4(NCS)_2$ and $Ru_2Cu(dpa)_4(NCS)_2$ are compared in Figure 5, while the voltage dependence of the transmission spectra is summarised in the stack plots in Figure 6. The $Ru_2Cu(dpa)_4(NCS)_2$ system provides a convenient reference point for the discusson because in this case current flow in both forward and reverse directions is dominated by the π* channels. Under forward bias the current is carried almost entirely by the spin-β component of the π* channel (spin-filtering efficiency, $\left(I^{\beta} - I^{\alpha}\right)/\left(I^{\beta} + I^{\alpha}\right) \times 100\% = 98\%$). This channel is localised primarily on the $\{Ru_2\}$ subunit and so it tracks the Fermi level of the right hand electrode, entering the bias window from above at +0.1 V (Figure 6). The forward current reaches a plateau value of ~ 1.0 μA at ~ +0.3 V and then continues to rise slightly as the bias increases further. The reverse bias current, in contrast, is dominated almost entirely by the spin-α component of the π* channel, which lies *below* the Fermi level at equilibrium and enters the bias window at –0.4 V. The current again reaches a plateau of ~1.0 μA but then, in contrast to the forward current, tails off at more negative bias. The similar plateau currents in forward and reverse direction correlate with the similar intensities of the π^*_{α} and π^*_{β} peaks in the transmission spectrum which, in turn, reflect their very similar degrees of left-right delocalisation. The different gradients of the current at higher voltages can also be tracked to the delocalisation of the channel, and specifically now to its dependence on bias. Forward bias stabilises the $\{Ru_2\}$ side of the molecule relative to Cu, and so the zeroth order separation between the orbitals in Scheme 1 (ΔE_1, ΔE_2) is reduced, leading to greater delocalisation. Conversely, reverse bias stabilises the Cu side, increasing the zeroth order energy gaps and reducing delocalisation. These trends are apparent in Figure 6(a), where the π* channels (both α and β) *increase* in intensity on going from left (reverse bias) to right (forward bias). Under forward bias the current-carrying channel therefore becomes *more* transparent as voltage increases whereas under reverse bias the channel closes off, giving a weak negative differential resistance (NDR) feature.

Turning to the $Ru_2Ni(dpa)_4(NCS)_2$ analogue, the forward current

is again entirely dominated by the π^*_β channel, and plateaus at ~ 5 μA before increasing further at higher voltage. The 5-fold increase in plateau current compared to $Ru_2Cu(dpa)_4(NCS)_2$ is a direct result of the spin polarisation of the $d_{xz/yz}$ levels on Ni which enhances the left-right delocalisation of the π* β channel and raises the intensity of the corresponding transmission peak. The behaviour under reverse bias is more complicated because there are now significant contributions to the current from both spin-α and spin-β manifolds. The spin-α current is again carried by the π* channel, which plateaus at ~2 μA before tailing off to higher bias for exactly the same reasons as discussed above. In the absence of the spin-β component of the current, therefore, the π* manifold could support a rectification ratio of ~3.0 at biases in excess of 1 V. In the present case, however, the rectification is compromised by the presence of a substantial spin-β component carried by the σ^{nb} channel, which also enters the bias window at -0.5 V (Figure 6b).

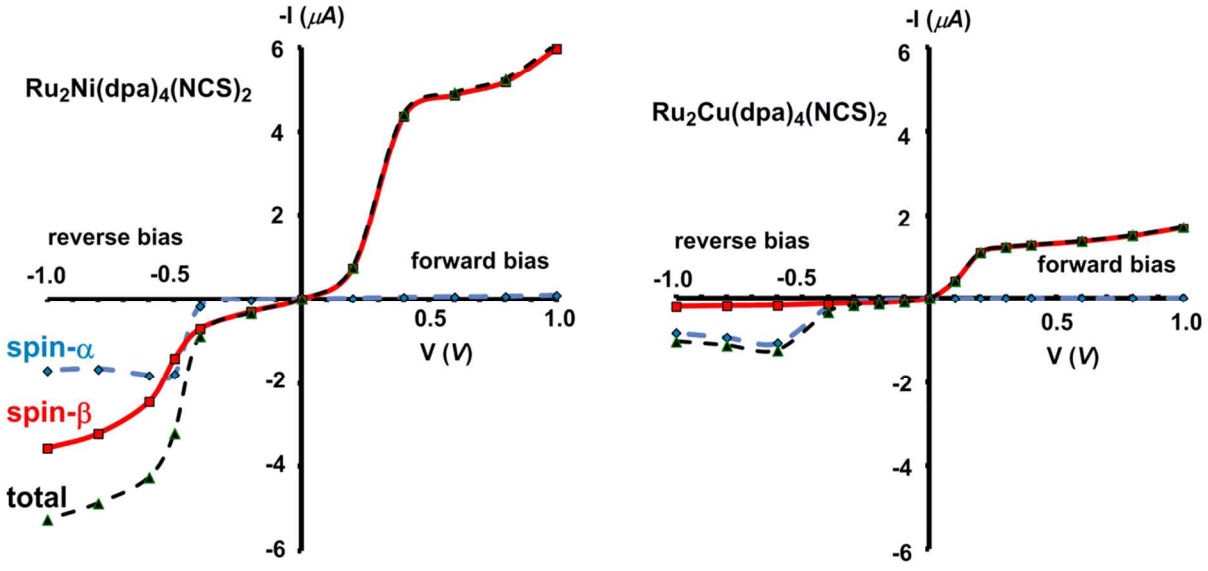

Figure 5. Computed current-voltage characteristics for $Ru_2Ni(dpa)_4(NCS)_2$ and $Ru_2Cu(dpa)_4(NCS)_2$ Forward bias is defined where $V_R > V_L$ (*i.e.* $E_{fR} < E_{fL}$ and the flow of electrons is from Ni to Ru)).

Cite this: DOI: 10.1039/c0xx00000x

www.rsc.org/xxxxxx

ARTICLE TYPE

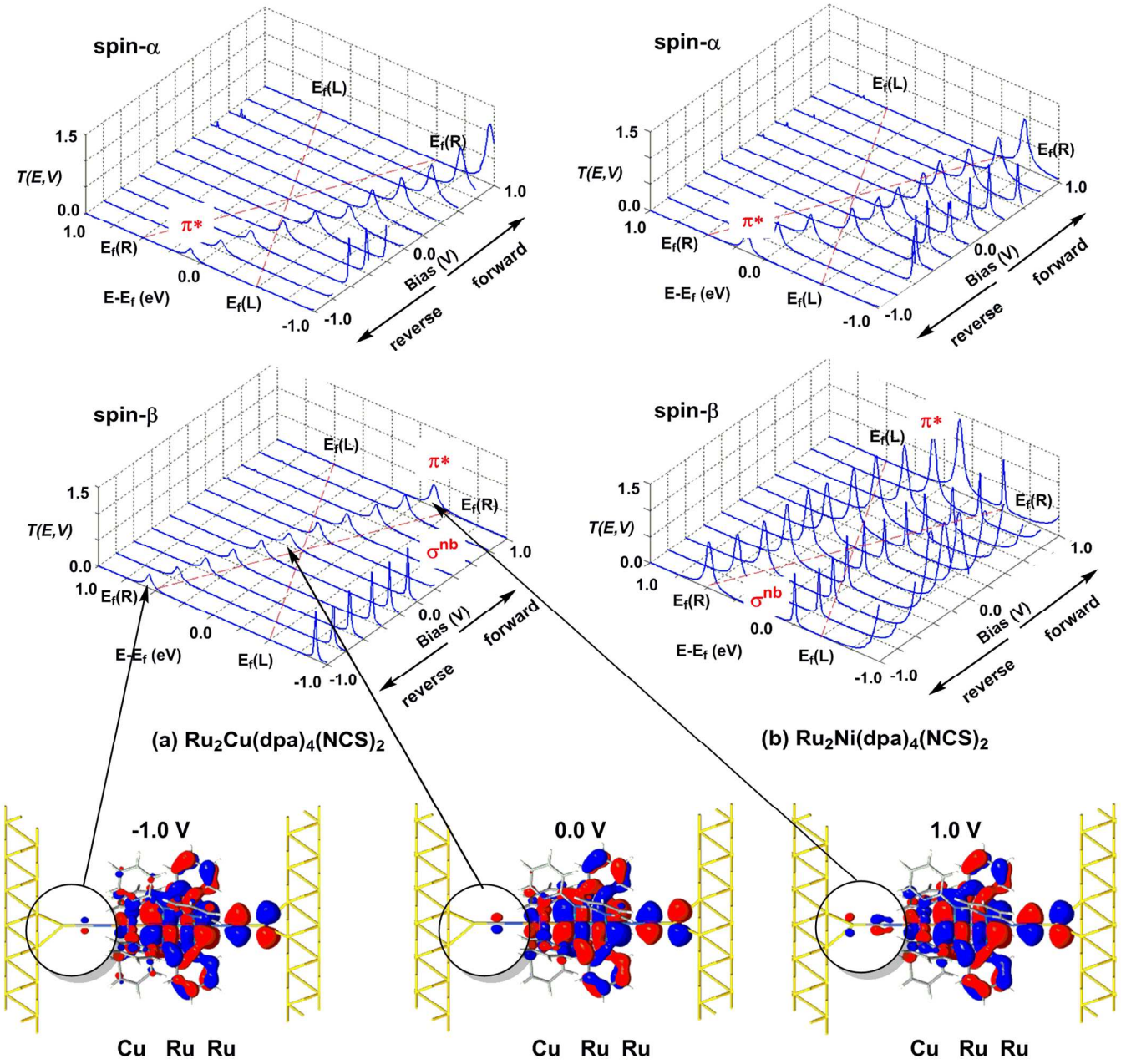

Figure 6. Voltage dependence of transmission spectra of (a) $Ru_2Cu(dpa)_4(NCS)_2$ and (b) $Ru_2Ni(dpa)_4(NCS)_2$. Isosurface plots for the π^*_β channel of $Ru_2Cu(dpa)_4(NCS)_2$ at equilibrium and under forward and reverse bias (±1.0 V), highlighting the increasing left-right delocalisation under forward bias. The bias window is indicated by dashed red lines.

Conclusions and outlook

The arguments set out in this paper identify the features of electronic structure that can lead to asymmetric current flow. Physical asymmetry of the kind present in both $Ru_2Ni(dpa)_4(NCS)_2$ and $Ru_2Cu(dpa)_4(NCS)_2$ is a necessary condition for rectification, but is not sufficient to guarantee substantial rectification ratios. There are in fact three distinct features of the system that combine to afford the observed rectification. (1) the presence of a spin moment, which displaces

the spin-α and spin-β components of the π* channel below and above the Fermi, respectively. (2) the localisation of the channel on the Ru_2 unit, which means that the current is always limited by the rate of entry/escape from the left hand electrode to the Ni/Cu end of the molecule. This localisation also ensures that both spin components track the potential of the right hand electrode, with the result that the spin-β and spin-α channels carry current under forward and reverse bias, respectively. (3) The presence of a paramagnetic heteroatom (Ni) which tunes the left-right delocalisation of the spin-α and spin-β channels to different extents. The result is that the Au-SCN-Ni junction is more transparent to spin-β electrons than to spin-α, giving a larger current under forward bias. Whilst the calculated rectification ratios are small in these particular systems, the model presented here provides a set of underlying principles that can underpin the rational design of molecules with improved functionality.

Acknowledgements
We acknowledge the EPSRC (UK) for financial support (EP/K021435/1)

Notes and references

[a] *Department of Chemical Physics, University of Science and Technology of China, Hefei, Anhui 230026, China. Fax: +86 0594 3393225; Tel: +86 1878 8836368; E-mail: titi@mail.ustc.edu.cn* [b]*Department of Chemistry, University of Oxford, South Parks Road, Oxford, OX1 3QR, UK. Fax: +44(0)1865 272; Tel: +44(0)1865 272645; E-mail: john.mcgrady@chem.ox.ac.uk*

† Electronic Supplementary Information (ESI) available: [details of any supplementary information available should be included here]. See DOI: 10.1039/b000000x/

1 (a) G. C. Solomon, C. Herrmann and M. A. Ratner, *Top. Curr. Chem*., 2012, **313**, 1. (b) J. Jortner, A. Nitzan and M. A. Ratner in '*Introducing Molecular Electronics'*, Springer (Heidelberg), 2005. (c) A. R. Rocha, V. M. Garcia-Suarez, S. W. Bailey, C. J. Lambert, J. Ferrer and S. Sanvito, *Nature Mat*., 2005, **4**, 335. (d) W. Y. Kim, Y. C. Choi, S. K. Min, Y. Cho and K. S. Kim, *Chem. Soc. Rev*., 2009, **38**, 2319.

2 K. Stokbro, J. Taylor and M. Brandbyge, *J. Am. Chem. Soc*., 2003, **125**, 3674.

3 D. DeBrincat, O. Keers and J. E. McGrady, *Chem. Commun*., 2013, **49**, 9116.

4 R. M. Metzger and D. Mattern, *Top. Curr. Chem*., 2012, **313**, 39. (b) T. Zu, I. R. Peterson, M.V. Lakshmikantham and R. M. Metzger, *Angew. Chem. Int. Ed., Engl*., 2001, **40**, 1749.

5 G. J. Ashwell, J. R. Sambles, A. S. Martin, W. G. Parker and M. Szablewski, *J. Chem. Soc., Chem. Commun*., 1990, 1374.

6 R. Stadler, V. Geskin and J. Cornil, *J. Phys., Condens. Matter*, 2008, **20**, 374105. (b) R. Stadler, V. Geskin and J. Cornil, *Adv. Funct. Mat*., 2008, **18**, 1119.

7 (a) A. Troiisi and M. A. Ratner, *J. Am. Chem. Soc*., 2002, **124**, 14528. (b) A. Troisi and M. A. Ratner, *Nano Lett*., 2004, **4**, 591.

8 A. Batra, P. Darancet, Q. Chen, J. S. Meisener, J. R. Widawsky, J. B. Neaton, C. Nuckolls and L. Venkataraman, *Nano Lett*., 2013, **12**, 6233.

9 (a) A. Staykov, D. Nozaki and K. Yoshizawa, *J. Phys. Chem. C*, 2007, **111**, 11699. (b) Y. Tsuji, A. Staykov and K. Yoshizawa, *J. Phys. Chem. C*, 2012, **116**, 2575. (c) Y. Tsuji and K. Yoshizawa, *J. Phys. Chem. C*, 2012, **116**, 26625. (d) A. Staykov, X. Li, Y. Tsuji and K. Yoshizawa, *J Phys. Chem. C*, 2012, **116**, 18451. (d) A. Staykov and P. Tzenov, *J. Phys. Chem. C,* 2013, **117**, 13644.

10 (a) Y. Min, J. H. Fang, C. G. Zhong, Z. C. Dong, C. P. Chen and K. L. Yao, *Comp. Mat. Sci*., 2014, **81**, 418. (b) L. Zhu, K. L. Yao and Z. L. Liu, *Chem. Phys*., 2012, **397**, 1.

11 Z. Li, J. Zheng, Z. Ni, R. Quhe, Y. Wang, A. Gao and J. Lu, *Nanoscale*, 2013, **5**, 6999.

12 (a) H. Liu, H. Wang, J. Zhao and M. Kiguchi*, J. Comput. Chem*., 2013, **34**, 360. (b) H. Liu, N. Wang, P. Li, X. Yin, C. Yu, N. Gao and J. Zhao, *Phys. Chem. Chem. Phys*., 2011, **13**, 1301. (c) H. Liu, J. Zhao, F. Boey and H. Zhang, *Phys. Chem. Chem. Phys*., 2009, **11**, 10323.

13 Z. Li and D. S. Kosov, *J. Phys. Chem. B*, 2006, **110**, 9893.

14 J. Zhao, C. Zeng, X. Cheng, K. Wang, G. Wang, J. Yang, J. G. Hou and Q. Zhu, *Phys. Rev. Lett*., 2005, **95**, 045502.

15 A. Aviram and M. A. Ratner, *Chem. Phys. Lett*., 1974, **29**, 277.

16 (a) A. Soncini, T. Mallah and L. F. Chibotaru, *J. Am. Chem. Soc*., 2010, **132**, 8106. (b) L. A. Zotti, E. Leary, M. Soriano, J. C. Cuevas and J. J. Palacios, *J. Am. Chem. Soc*., 2013, **135**, 2052. (c) Q.-Q. Sun, Y.-J. Li, J. -L. He, W. Yang, P. Zhou, H. -L. Lu, S. -J. Ding and D. W. Zhang, *App. Phys. Lett*., 2013, **102**, 093104. (d) Y. Matsuura, *J. Chem. Phys*., 2013, **138**, 014311. (e) H. Hao, X. Zheng, Z. Dai and Z. Zeng, *J. App. Phys*., 2011, **110**, 023702.

17 J. F. Berry, *Structure and Bonding*. 2010, 136 . (b) J. F. Berry in: F. A. Cotton, C. A. Murillo, R. A. Walton (Eds.), *Multiple Bonds Between Metal Atoms,* Springer, New York, USA, 2005. (c) C. -Y. Yeh, C. -C. Wang, C. –h. Chen, S. -M. Peng, in: T. Hirao, *Redox Systems Under Nano-Space Control*, Ed., Springer, Berlin, 2006.

18 C. Herrmann, G. C. Solomon and M. A. Ratner, *J. Am. Chem. Soc*., 2010, **132**, 3682.

19 Y. Tsuji, A. Staykov and K. Yoshizawa, *J. Phys. Chem C*, 2012, **116**, 16325.

20 K. -N. Shih, M. -J. Huang, H. -C. Lu, M. -D. Fu, C. -K. Kuo, G. -C. Huang, G. -H. Lee, C. -h. Chen and S. -M. Peng, *Chem. Commun*., 2010, **46**, 1338.

21 (a) S. -Y. Lin, I. -W. P. Chen, C. -h. Chen, M. -H. Hsieh, C. -Y. Yeh, T. -W. Lin, Y. -H. Chen, S. -M. Peng, *J. Phys. Chem. B*., 2004, **108**, 959. (b) I. -W. P. Chen, M. -D. Fu, W. -H. Tseng, J. -Y. You, S. -H. Wu, C. -J. Ku, C. -h. Chen, S. -M. Peng, *Angew. Chem. Int. Ed*., 2006, **45**, 5814.

22 I . P. -C. Liu, M. Bénard, H. Hasanov, I. -W. P. Chen, W.- H. Tseng, M. -D. Fu, M. -M. Rohmer, C. -h. Hsien, G. -H. Lee and S. -M. Peng, *Chem. Eur. J*., 2007, **31**, 8667.

23 (a) V. P. Georgiev and J. E. McGrady, *Inorg. Chem*. 2010, **49**, 5591. (b) V. P. Georgiev and J. E. McGrady, *J. Am. Chem. Soc*. 2011, **133**, 12590. (c) V. P. Georgiev, W. M. C. Sameera and J. E. McGrady, J. Phys. Chem. C, 2012, **116**, 20163. (d) V. P. Georgiev, P. J. Mohan and J. E. McGrady, *Chem. Sci*., 2012, **3**, 1319. (e) V. P. Georgiev, P. J. Mohan, D. DeBrincat and J. E. McGrady, *Coord. Chem. Rev*., 2013, **257**, 290.

24 Y. Kitagawa, T. Matsui, Y. Nakanishi, Y. Shigeta, T. Kawakami, M. Okumura and K. Yamaguchi, *Dalton Trans*., 2013, **42**, 16200.

25 D. A. Luzhbin, S. S. Kaun, E. A. Bondar, *Metallofisika i Noveishie Tekhnologii*, 2008, **30**, 19.

26 (a) L. Y.; Hsu, Q. -R. Huang and B. -Y. Jin, *J. Phys. Chem. C*. 2008, **112**, 10538 (b) T.W. Tsai, Q. -R. Huang, S. -M. Peng and B. -Y. Jin, *J. Phys. Chem*. C 2010, **114**, 3641.

27 G. -C. Huang, M. Bénard, M. -M. Rohmer, L. -A. Li, M. -J. Chiu, C. -Y. Yeh, G. -H. Lee and S. -M. Peng, *Eur. J. Inorg. Chem*., 2008, **11**, 1767.

28 (a) G. te Velde, F. M. Bickelhaupt, S. J. A. van Gisbergen, C. Fonseca Guerra, E. J. Baerends, J. G. Snijders and T. Ziegler, *J. Comp. Chem*. 2001, **22**, 931. (b) C. Fonseca Guerra, J. G. Snijders, G. te Velde and E. J. Baerends, E.J. *Theor. Chem. Acc*. 1998, **99**, 391 (c) ADF2012, SCM, Theoretical Chemistry, Vrije Universiteit, Amsterdam, The Netherlands, http://www.scm.com.

29 R. G. Parr and W. Yang, W. Density Functional Theory of Atoms and Molecules, Oxford University Press, Oxford, 1989.

30 S. H.Vosko,L. Wilk and M. Nusair, *Can. J. Phys*. 1980, **58**, 1200.

31 J. P. Perdew, K. Burke and M. Ernzerhof, *Phys. Rev. Lett*., 1996, **77**, 3865.

32 http://www.quantumwise.com/

33 (a) M. Brandbyge, J. –L. Mozos, P. Ordejon, P. Taylor, and K. Stokbro, Phys. Rev. B. 2002, **65**, 165401. (b) J. M. Soler, E.

Artacho, J. D. Gale, A. Garcia, J. Unquera, P. Ordejon and D. Sanchez-Portal, *J. Phys.: Condensed Matte*r 2002, **14**, 2745. (c) J. Taylor, H. Guo and J. Wang, *Phys. Rev. B*. 2001, **63**, 245407.
34 J. P. Perdew and A. Zunger,. *Phys. Rev*. B 1981, **23**, 5048.
35 (a) S. Datta, Electron Transport in Mesoscopic Systems; Cambridge University Press, Cambridge, UK, 1997. (b) S. Datta, Quantum Transport: Atom to Transistor, Cambridge University Press, Cambridge, UK, 2005. (c) S. Lindsay, *Farad. Disc*. 2006, **131**, 403. (d) R. H. Smit, Y. Noat, C.. Untiedt, N. D. Lang, M. C. van Hemert And J. M. van Ruitenbeek, *Nature* 2002, **419**, 906. (f) L. H. Yu, Z. K. Keane, J. W. Ciszek, L. Cheng, M. P. Stewart, J. M. Tour and D. Natelson, *Phys. Rev. Lett*. 2004, **93**, 266802.
36 C. Toher C and S. Sanvito, *Phys. Rev. B* 2008, **77**, 155402.
37 (a) R. Cohen, K. Stokbro, J. M. L. Martin, and M. A. Ratner, *J. Phys. Chem. C* 2007, **111**, 14893. (b) H. Liu, C. Yu, N. Gao and J. Zhao, *ChemPhysChem* 2010, **11**, 1895. (c) K. Tagami and M. Tsukuda, *J. Phys. Chem*. B 2004, **108**, 6441.
38 N. Troullier and J. L. Martins, *Phys. Rev. B* 1991, **43**, 1993.
39 H. J. Monkhorst and J. D. Pack, *Phys. Rev. B* 1976, **13**, 5188.
40 M. Buttiker, Y. Imry, R. Landauer and S. Pinhas, *Phys. Rev. B*, 1985, **31**, 6207.